Time-frequency analysis of light-bullet dynamics during femtosecond filamentation in the anomalous dispersion regime

Ya Tian,[1,2] Cheng Gong,[2,*] Xiangming Hu,[1] and XiaoJun Liu[2,†]
[1]*College of Physical Science and Technology, Central China Normal University, Wuhan 430079, China*
[2]*State Key Laboratory of Magnetic Resonance and Atomic and Molecular Physics, Wuhan Institute of Physics and Mathematics, Innovation Academy for Precision Measurement Science and Technology, Chinese Academy of Sciences, Wuhan 430071, China*

(Received 26 February 2021; accepted 20 September 2021; published 8 October 2021)

In this paper, we investigate the light-bullet dynamics during femtosecond laser filamenation in an anomalous dispersion regime based on the experimentally observed blueshifted resonant radiation (RR) in fused silica. A numerical simulation is performed and well reproduces the pronounced asymmetric feature of the RR spectra. By applying a time-frequency analysis to the propagating laser field, this specific spectral feature is found to be closely connected to the positively chirped property of RR in the time domain. In the context of the effective three-wave mixing model, this temporal chirp character of the RR is ascribed to the variable phase-matching conditions, which can be traced back to the accelerative propagation of the light bullet during its formation. Our work provides a deep understanding of the spatiotemporal dynamics of femtosecond laser-pulse propagation in condensed media.

DOI: 10.1103/PhysRevA.104.043506

I. INTRODUCTION

Optical solitons are of fundamental importance in modern optics due to their applications in optical data transmission [1], fiber-laser technologies [2,3], and light generation at new frequencies [4,5]. Meanwhile, optical solitons can also be used as a prototype to investigate novel phenomena ranging from the optical analogy of an event horizon [6] and wave trapping [7] to rogue waves [8]. Therefore, generation of an optical soliton and understanding its propagation dynamics have attracted a great deal of interest in fundamental and applied research [9]. The fiber soliton (one spatial dimension and one temporal dimension, 1+1D) has been extensively studied [10,11] since it was predicted and demonstrated four decades ago [12,13]. Until recently, it becomes possible to investigate the real-time dynamics of the optical soliton in fiber [3,14] after a powerful method of dispersive Fourier transformation [15] has been applied. However, the generation of three-dimensional spatiotemporal solitons (also called light bullets), which propagate in the medium without natural dispersive broadening and diffractive spreading [16], is still nontrivial work, for it requires accurate control of the optical pulse propagation in a medium in both the spatial and temporal domains simultaneously.

Recently, femtosecond laser filamentation at midinfrared laser wavelengths provided the ability to generate a light bullet [17–20]. In general, the physical mechanism behind the filamentation process can be ascribed to a dynamic balance between the self-focusing effect due to the optical Kerr effect and defocusing effects resulting from ionization-induced plasma [21] and/or high-order Kerr effects [22]. This dynamic balance leads to a spatially invariant laser intensity distribution over a long propagation distance [23], which can be viewed as a one-dimensional (1D) quasispatial soliton. Only when the laser wavelength lies in the anomalous dispersion region does the interplay between self-action effects and anomalous group-velocity dispersion (GVD) make it possible to compress the pulsed laser beam in both spatial and temporal domains simultaneously, and as a result, a three-dimensional spatiotemporal soliton, or a light bullet, is formed [17,20].

Up to now, numerous experimental and theoretical studies have shown a host of phenomena that are accompanied by the formation of a light bullet, such as the generation of an ultrabroadband supercontinuum [24–26], conical emissions [27], third-harmonic generation [28], and generation of optical negative frequency [5,29]. These associated spectral features not only provide various potential applications of light bullets [30,31] but also may be applied to retrieve the propagation dynamics of the light bullet, e.g., by using an effective three-wave mixing (ETWM) model [32,33]. In particular, a blueshifted spectral peak [termed resonant radiation (RR)] in the visible region of the supercontinuum generated during femtosecond filamentation in the anomalous dispersion region can be viewed as an indication of the generation of a light bullet [27,33], and the wavelength of the RR spectral peak has been applied to retrieve the velocity of the light bullet after it has been generated [27,34]. However, although some properties of light bullets have been successfully obtained, the formation dynamics of light bullets during femtosecond laser filamentation is still far from understood, partly due to

*gongcheng@wipm.ac.cn
†xjliu@wipm.ac.cn

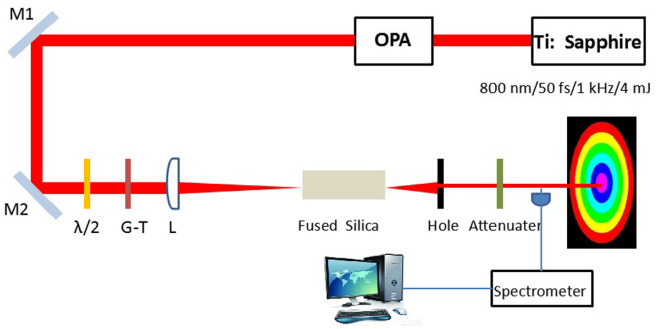

FIG. 1. Schematic representation of our experimental setup for femtosecond laser filamentation in fused silica: OPA, optical parametric amplifier; M1, M2, silver mirrors; $\lambda/2$, half-wave plate; G-T, Glan-Taylor polarizer; L, plano-convex lens; Hole, an aperture; Attenuator, different neutral filters.

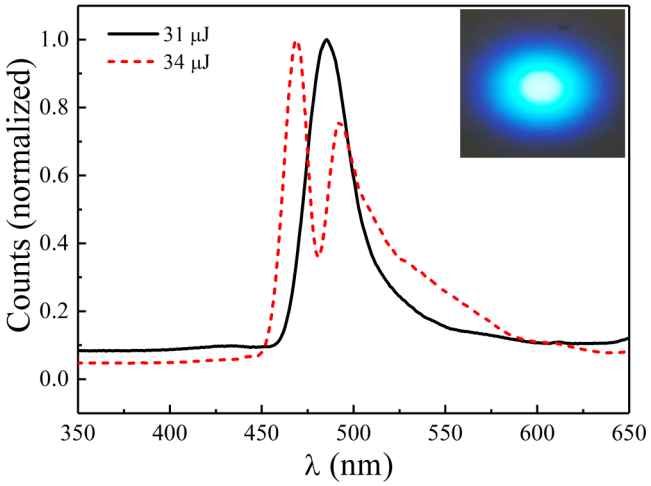

FIG. 2. Spectra in the visible region measured on the laser propagation axis; the black solid line (red dashed line) corresponds to input pulse energy of 31 μJ (34 μJ). The inset shows the conical emission at 31 μJ.

the lack of an effective analysis method to get inside the laser propagation dynamics.

With this in mind, the purpose of the present work is to offer an analysis method to retrieve the light-bullet formation dynamics based on the experimentally observed blueshifted RR spectrum during midinfrared femtosecond laser filamentation in fused silica. Thus, we first numerically simulate the laser-pulse propagation in the sample and obtain the spatiotemporal distribution of the laser beam along its propagation direction. Thereafter, a time-frequency analysis is applied to the propagation laser fields to uncover in detail the characteristics of the RR spectrum. It is found that the pronounced asymmetric spectral feature of RR, extensively observed in experiments, is closely related to its positively chirped property in the time domain. Furthermore, according to an analysis using the ETWM model, this temporal chirp character of the RR is ascribed to the variable phase-matching conditions, which can be traced back to the accelerative propagation of the light bullet during its formation. Our work demonstrates in detail how the RR spectrum is formed along the propagation of the laser field in the medium and thus provides deep understanding of the spatiotemporal dynamics of femtosecond laser-pulse propagation in condensed media.

II. EXPERIMENTAL SETUP AND RESULTS

The experimental setup is depicted schematically in Fig. 1. An optical-parametric-amplification laser system pumped by a commercial Ti:sapphire laser amplification system (Coherent Legend HE+, 1 kHz, 5 mJ, 800 nm) can deliver laser pulses with the wavelength tunable from 1.1 to 2.6 μm. In our experiments, the central wavelength of the driving laser is 2.08 μm, falling in the negative GVD region of fused silica, and the pulse duration (FWHM) is about 70 fs. As shown in Fig. 1, M1 and M2 are silver mirrors, and the combination of a half-wave plate and a Glan-Taylor polarizer is employed to adjust the laser-pulse energy injected into the sample. Thereafter, laser pulses are focused with a 40-cm plano-convex lens with its focus at the rear face of a 2-cm-long fused silica cuboid. In our work, we focus on the temporal and spectral structures of the on-axis component of the laser field. Therefore, downstream of the sample, the generated spectrum on the axis is chosen by an aperture with a diameter of 300 μm. To avoid spectral saturation of the spectrometer, neutral filters (Thorlabs, NEK01) are selected to properly attenuate the spectral intensity, and the spectra are recorded using a fiber spectrometer with a 16-bit dynamic range detector (QE6500, Ocean Optics), covering a wavelength range from 0.35 to 1.1 μm.

In the experiment, the laser-pulse energy is finely adjusted by rotating the half-wave plate. In Fig. 2 we show the axial spectrum recorded by the spectrometer with an integral time of 200 ms. As the laser-pulse energy is gradually increased to 30 μJ, a weak conical emission begins to appear after the sample, as shown in the inset of Fig. 2, which can be considered an indication of the formation of a filament in the medium [27,35,36]. The input laser-pulse energy is thus chosen to be 31 μJ, which is just a little above the threshold for filamentation in our experiment. A blueshifted spectral peak in the visible region is observed, as shown by the black solid line in Fig. 2, and the wavelength corresponding to the maximal intensity (termed the peak wavelength hereafter) is about 483 nm. Note that this spectral peak exhibits an asymmetric feature with wider spectra on the longer wavelength side, which has also been observed in previous experiments [26,27,31]. It is also worth mentioning that this blueshifted spectral peak can be observed in only a narrow range of input laser-pulse energies. Specifically, when the input energy is further increased to 34 μJ, this spectral peak is split into two peaks, as shown by the red dashed line in Fig. 2. In this situation, two filaments are generated along the propagation direction, and each filament generates a set of supercontinua, which will interfere with each other outside the sample [36]. As a result, the single blueshifted spectral peak will split into two peaks. In our work, we focus on just the case of the generation of a single blueshifted spectral peak.

Note that previous studies have been done on this blueshifted spectral peak [27,36], and the appearance of RR was interpreted by the ETWM model [32]. Within this model, for a range of driving laser power above the critical power

for self-focusing, the laser pulse undergoes filamentation and does not split in the time domain due to self-phase modulation (SPM) in conjunction with anomalous group-velocity dispersion. As a result, a light bullet is formed, and the laser beam remains the profile of a single peak with a propagation velocity v_p which can be larger or smaller than the group velocity v_g of the incident laser pulse. This light bullet generates a traveling perturbation of the refractive index acting as a polarization wave with a frequency of $\omega - \omega_0$, which in turn scatters the incident laser pulse of frequency ω_0. This scattering process is associated with a phase-matching condition,

$$\Delta k = k_z(\omega, k_\perp) - k_0 - \frac{\omega - \omega_0}{v_p}, \tag{1}$$

where k_z is the wave vector propagating along the propagation direction and $k_\perp$ is the transverse wave vector. The above equation indicates that the phase-matching condition can be fulfilled only around a certain wavelength, which leads to the generation of a peak structure in the spectrum. This blueshifted spectral peak is thus termed resonant radiation, which is well known during the generation of a soliton in an optical fiber [37,38]. After fitting the peak wavelength of the experimental results in Fig. 2 with Eq. (1), the propagation velocity v_p of the light bullet is $1.0019 v_g$, where v_g is the group velocity of the input laser pulse in fused silica. However, the above-mentioned model gives only the peak wavelength of the RR, and as far as we know, little attention has been paid to the asymmetric feature of RR which involves abundant dynamic information about the laser-pulse propagation in the medium. We will focus on this asymmetric feature and uncover its origin in what follows.

III. NUMERICAL SIMULATION AND DISCUSSION

In order to simulate the spatiotemporal dynamics of femtosecond laser pulses and the accompanying RR formation during filamentation in fused silica, the unidirectional pulse propagation equations (UPPEs) [39] are applied. In the moving frame $\tau = t - z/v_g$, where t denotes time in the laboratory frame, the evolution of the z-propagated complex laser-pulse envelope $\widetilde{E}(\omega, k_\perp, z)$ in the spectral domain satisfies

$$\frac{\partial \widetilde{E}}{\partial z} = i\mathcal{K}(k_x, k_y, \omega)\widetilde{E} + i\mathcal{Q}(\omega)\left(\frac{\widetilde{P}}{\varepsilon_0} + \frac{i}{\omega}\frac{\widetilde{J}}{\varepsilon_0}\right). \tag{2}$$

Here the first term on the right-hand side represents diffraction, dispersion, and space-temporal coupling: $\mathcal{K}(k_x, k_y, \omega) = k(\omega) - \kappa(\omega) + \Delta_\perp/2k(\omega)$, where the dispersive properties of the medium are described by a Sellmeier-like relation $k(\omega)$ [40], and $\kappa(\omega) = k_0 + (\omega - \omega_0)/v_g$. The nonlinear dispersion reads $\mathcal{Q}(\omega) = \frac{1}{2}k(\omega)^{-1}\omega^2/c^2$. In addition, the nonlinear source terms in the equation include a nonlinear polarization $P(t, r, z)$ and a nonlinear current source $J(t, r, z)$, which are computed in the time domain. In detail, the nonlinear polarization describes the optical Kerr effect

$$\frac{P}{\varepsilon_0} = 2n_0 n_2 |E|^2 E, \tag{3}$$

and the current which represents plasma absorption and plasma defocusing in the framework of the Drude model is governed by

$$\frac{J}{\varepsilon_0} = c\sigma_0(1 + i\omega_0\tau_c)\rho E + cn_0\beta_K|E|^{2K-2}E, \tag{4}$$

where c is the speed of light in a vacuum, ω_0 is the central frequency of the laser pulse, n_0 and n_2 are the linear and nonlinear refractive indexes, respectively, σ_0 is the cross section for inverse bremsstrahlung, τ_c is the effective collision time, ρ is the density of electrons generated by ionization, β_K denotes the cross section for multiphoton absorption (MPA), $K \equiv \langle (U_g/\hbar\omega_0) + 1 \rangle$ ($\langle \cdots \rangle$ represents the integer part) denotes the number of photons involved in the multiphoton process, and U_g is the band gap of the material. In our simulation, multiphoton ionization (MPI), avalanche ionization (AI), and the recombination process are considered, and the evolution equation of the free electrons is

$$\frac{\partial \rho}{\partial t} = \sigma_K|E|^{2K}(\rho_{nt} - \rho) + \sigma_0|E|^2\frac{\rho}{U_g} - \frac{\rho}{\tau_r}, \tag{5}$$

where σ_K is the cross section for MPI, ρ_{nt} is the density of neutral molecules, and τ_r denotes the characteristic time for recombination. Among these parameters, σ_K is obtained from a complete Keldysh formulation, i.e., Eq. (37) in Ref. [41], β_K is calculated by the relation $\beta_K = \sigma_K \times K\hbar\omega_0\rho_{nt}$, and σ_0 follows the Drude model [21], which reads

$$\sigma_0 = \frac{e^2}{\epsilon_0 m_e c n_0}\frac{\tau_c}{1 + \omega_0^2\tau_c^2}. \tag{6}$$

Note that, in our model, the strong field-induced Stark effect in solids [42,43] has been neglected since it plays a minor role and normally cannot be extracted in femtosecond laser filamentation [21,39]. The other parameters of the nonlinear medium used in the simulation are provided in Table I. The input driving laser field is assumed to be Gaussian in both the temporal and spatial domains with a central wavelength of 2.08 μm, a pulse duration of 70 fs (FWHM), and a waist of 100 μm.

As shown in Fig. 3(a), during femtosecond laser-pulse propagation in fused silica, the on-axis laser intensity increases gradually due to the Kerr self-focusing effect. Meanwhile, in the spectral domain, new redshifted (blueshifted) spectra are generated on the ascending (descending) part of the pulse by the SPM effect, which leads to laser-pulse spectral broadening symmetrically. In the temporal domain, as the

TABLE I. Parameters for numerical simulation.

Quantity	Variable (units)	Value	Ref.
Refractive index	n_0	1.43	[10]
Kerr index coefficient	n_2 (cm^2/W)	2.3×10^{-16}	[44]
Band gap	U_g (eV)	9	[45]
Number of photons	K	16	
Cross section for MPA	β_{16} ($\mathrm{cm}^{29}/\mathrm{W}^{15}$)	6.42×10^{-192}	
Cross section for MPI	σ_{16} ($\mathrm{cm}^{32}/\mathrm{W}^{16}/\mathrm{s}$)	2×10^{-196}	
Collision time	τ_c (fs)	3	[46]
Recombination time	τ_r (fs)	150	[47]
Neutral density	ρ_{nt} (cm^{-3})	2.1×10^{22}	[46]
Cross section for AI	σ_0 (cm^2)	4.7×10^{-21}	

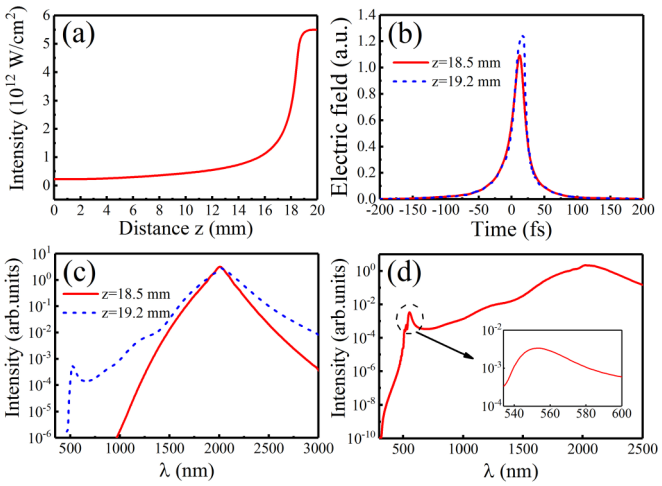

FIG. 3. Numerical simulation results. The intensity of the initial pulse is 3.5×10^{11} W/cm^2. (a) The axial intensity at different positions of the sample. (b) Electric-field envelope and (c) corresponding spectral intensity of the laser pulse after propagating at two positions of the medium. The red solid line (blue dashed line) represents the laser pulse arriving at 18.5 mm (19.2 mm). (d) The axial intensity spectrum at 20 mm; the inset displays an asymmetrical structure of RR.

driving laser wavelength falls in the anomalous dispersion region, new frequencies generated by SPM are swept back to the peak of the pulse. Consequently, a simultaneous temporal and spatial compression happens. During laser-pulse propagation in the medium, this compression is a runaway effect in the sense that as the beam self-focuses, the intensity increases dramatically, and so does the self-focusing effect. However, when the laser beam propagates close to the nonlinear focus around 18.0 mm, the laser intensity increases up to a certain level, and the strong field ionization begins to play an important role [48–50], which leads to an intensive energy loss and the generation of free-electron plasma. Consequently, the beam collapse is arrested by multiphoton absorption and defocusing of the plasma. The interplay of these effects clamps the intensity to a certain level after 18.5 mm, as shown in Fig. 3(a), and a light bullet will be generated, which can provide a steady phase-matching condition over a certain distance for RR generation. The generation of RR can be further understood by comparing the temporal electric-field envelope [Fig. 3(b)] and the corresponding spectra [Fig. 3(c)] of the propagating laser pulse at 18.5 mm and 19.2 mm. At the propagation position of 18.5 mm, the descending part of the laser pulse is very steep, but the RR has not yet been generated. This descending part of the laser pulse is due to the space-time focusing and self-steepening effects which originate from the interplay between the nonlinear effects and chromatic dispersion [21]. Consequently, a blue broadening spectrum [red solid line in Fig. 3(c)] is generated. However, these effects alone cannot lead to the appearance of RR because the spectra of the supercontinuum are not wide enough. In contrast, at a propagation position of 19.2 mm, RR spectra appear obviously in the visible region, as shown by the blue dashed line in Fig. 3(c). In this situation, an additional effect related to the free-electron plasma, which is generated by strong field ionization, can further cause a blueshift of the spectra and, meanwhile, clamps the laser intensity [21]. Thus, it is the interplay of all the SPM, self-steepening, and plasma effects that gives rise to the appearance of RR. After 19.2 mm the laser intensity becomes almost unchanged, and at the exit of the sample, an obvious asymmetric peak appears, as shown in the inset of Fig. 3(d), which resembles the experimental results in Fig. 2 very closely.

The above simulation results indicate that after the nonlinear focus and before the position where laser intensity is finally clamped, the spatiotemporal distribution of the laser pulse varies dramatically. Especially, a blueshifted spectral peak is generated, and a light bullet is formed. Such dramatic evolution of the laser beam was also reported in other bulk media [34,51]. In order to gain deeper insight into the temporal dynamical evolution of the laser pulse, we apply a time-frequency analysis (TFA) method to explore the spectral and temporal structure of the RR. The TFA has been widely used in studying ultrafast nonlinear processes such as the spectral dynamics of laser diodes [52], laser-induced molecular wave-packet dynamics [53], and high-order-harmonic generation [54–56]. It is a wavelet transform analysis of the electric field along its propagation direction in the sample and can be written as

$$A(t,\omega) = \int E(t')\sqrt{\omega}W(\omega(t-t'))dt' \tag{7}$$

where $W(\omega(t-t'))$ is the mother wavelet,

$$W(x) = \left(\frac{1}{\sqrt{\tau}}\right)e^{ix}e^{-\frac{x^2}{2\tau_0^2}}. \tag{8}$$

In the discussions below, in order to identify the detailed temporal distributions of the RR spectra and without loss of generality, we choose $\tau_0 = 10$ fs to perform the wavelet transform.

Figures 4(a)–4(d) display three-dimensional graphs of the modulus of the time-frequency profile of the laser electric field at four different propagation positions in the sample. In Fig. 4(a), when the propagation distance is 17.5 mm, the blueshifted spectra (from 1400 to 800 nm) correspond to a time domain ranging from −40 to 40 fs, which is just within the driving laser-pulse envelope. In this case, the propagation distance is shorter than the nonlinear focus length, as shown in Fig. 3(a), and the spectral broadening is mainly due to SPM. The high-frequency cutoff of the spectra is about 800 nm, which is longer than the RR wavelength in Fig. 3(d). Therefore, no RR is generated. As the laser pulse propagates to 18.8 mm, the laser intensity begins to increase intensively, as shown by the blue solid line in Fig. 5(a), which represents the on-axis intensity evolution along the propagation direction. In this situation, the spectrum is blueshifted to 380 nm, and a spectral peak near 500 nm begins to appear at the trailing edge of the laser pulse, as shown in Fig. 4(b). This spectral peak corresponds to the RR spectra, and its temporal distribution lasts longer than 80 fs. When the laser pulse propagates further to 19.2 mm, as shown in Fig. 4(c), the RR spectra extends much wider to 100 fs in the time domain. It is worth noting that the axial intensity of the laser pulse at 100 fs is very low at this propagation position, as shown in Fig. 3(b). Thus, the RR spectra at this position cannot be generated through

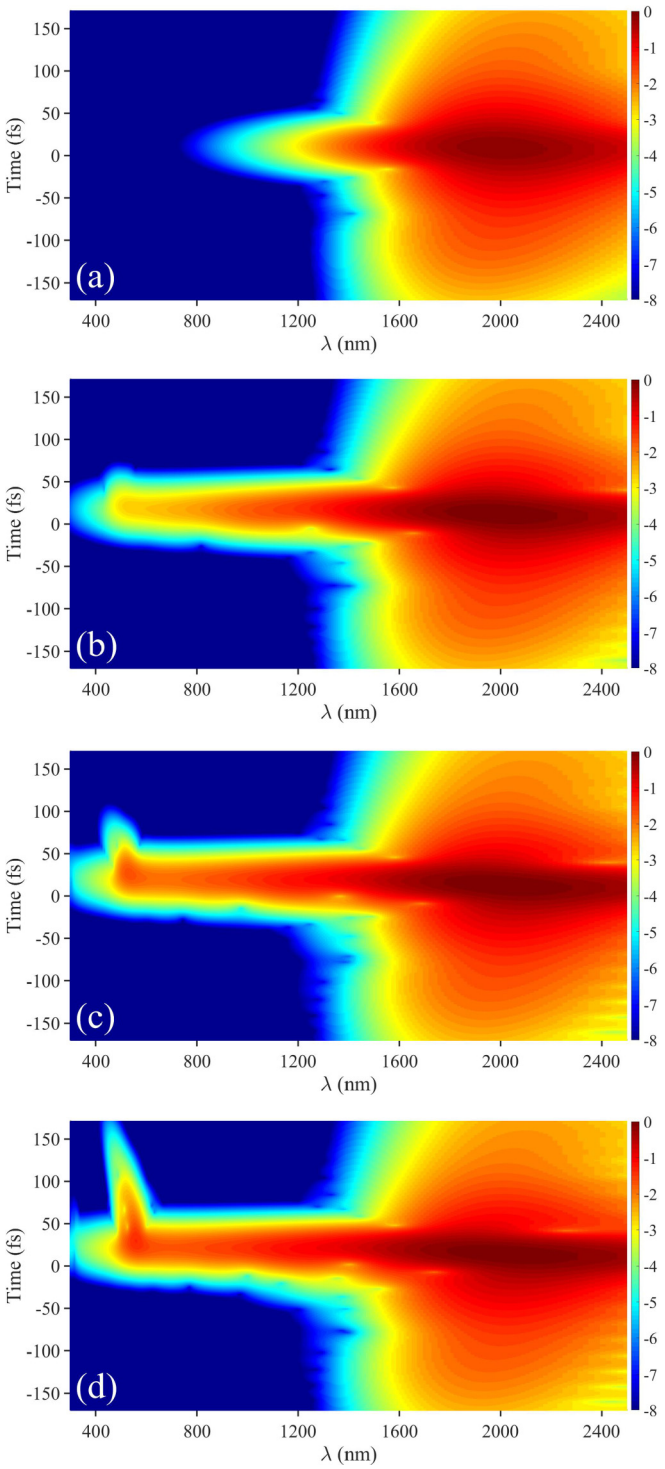

FIG. 4. Time-frequency spectra of the electric field propagating through the medium at (a) 17.5, (b) 18.8, (c) 19.2, and (d) 20 mm. The colors shown are in logarithmic scale.

SPM, self-steepening, or plasma effects. This suggests that the appearance of the RR spectra near 100 fs should be due to other causes, which can be ascribed to the group-velocity dispersion in the sample, as will be illustrated later. More interestingly, the wavelength of the RR peak varies at different times, and the RR peak exhibits a pronounced positive chirp, as shown in Figs. 4(b)–4(d). This temporal chirp property of

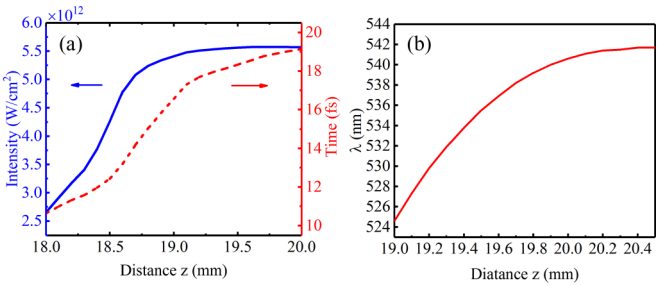

FIG. 5. (a) The laser intensity (blue solid line) and the time corresponding to the peak intensity (red dashed line) on the axis along with the propagation direction. (b) The calculated wavelengths of RRs at different propagation distances using the phase-matching condition according to Eq. (1).

the RR can be revealed only with the help of TFA. In addition, the laser intensity is still changing slowly and approaches being clamped, as shown in Fig. 5(a). When the laser pulse goes on propagating in the sample, the temporal distribution of the RR spectral peak extends to a wider and wider range. At the exit of the sample, as shown in Fig. 4(d), the wavelength of the spectral peak varies with time ranging from 20 to 180 fs. Consequently, this chirped property leads to the asymmetric structure of the RR spectrum.

Furthermore, this temporal chirped property of the RR, which has been revealed in our work and provides more insight into the laser propagation dynamics, can be understood with the ETWM model. In Eq. (1), it is assumed that the laser pulse propagates at a constant velocity. However, as shown in Fig. 5(a) (red dashed line), the peak position of the pulse in the time domain, which is obtained from the calculated on-axis laser pulse, varies nonlinearly along the laser propagation, indicating that the laser-pulse propagation velocity varies as it propagates in the sample. To be more specific, the laser-pulse propagation velocity in the laboratory frame is $v_p = (1/v_g + dt/dz)^{-1}$ [27], where v_g is the group velocity of the incident laser pulse and dt/dz is the slope of the red dashed line in Fig. 5(a). The slope dt/dz is related to the velocity of the RR moving within the pulse envelope, and it decreases with the increasing of propagation distance, which means that the driving pulse accelerates in the moving frame. In Fig. 5(b), we show RR peak wavelengths at different positions, which are calculated using Eq. (1), and the laser-pulse propagation velocities are retrieved from the red dashed line in Fig. 5(a). It is obvious that the increase of the laser-pulse propagation velocity leads to the generation of RR with a longer peak wavelength. This indicates that at different propagation positions, different RRs are generated. For example, at 19.2 mm, the pulse propagation velocity is $0.9989v_g$, and the peak wavelength of the RR is 530.2 nm, while the pulse propagation velocity increases to $0.9998v_g$ and the corresponding peak wavelength of RR becomes 538.6 nm at 19.8 mm.

Moreover, after the RR is generated at a certain position, further propagation of the RR in the local moving frame will lead to the specific chirp property of the RR shown in Fig. 4, which can be further understood in the following. Since the RR spectral wavelengths are near 500 nm, its group velocity is smaller than the group velocity of the incident laser pulse.

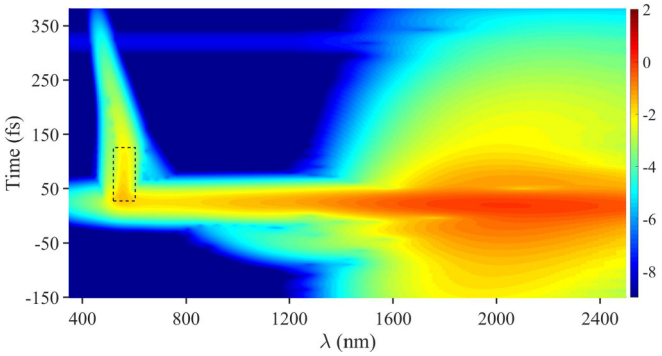

FIG. 6. Time-frequency spectra of the electric field propagating through the medium at 22 mm.

Thus, when a RR with peak wavelength λ_i is generated at a certain propagation position z_i, this RR will lag behind the driving pulse. The relative moving of the RR leads to the appearance of the spectra around 100 fs, as shown in Figs. 4(c) and 4(d), as mentioned in the preceding paragraph. This moving of the RR in the laser-pulse envelope can be described by the equation $t(z) = t(z_i) + (z - z_i)(1/v_{gi} - 1/v_g)$ [32], where z is the propagation position ($z > z_i$), $t(z_i)$ is the time at which the RR is generated, and v_{gi} and v_g are the group velocities of the RR and the incident laser pulse, respectively. From this equation, one can find that the moving of the RR in the laser-pulse envelope has a relative velocity of $(1/v_{gi} - 1/v_g)^{-1}$, which is a positive value. For RRs generated at different positions z_i, the time $t(z_i)$ is near 20 fs at the trailing edge of the laser pulse and changes very slowly, which can be assumed to be a constant. Compared with the RR generated at the later position, the RR generated at the earlier position has a shorter peak wavelength, as shown in Fig. 5(b); thus, this RR will propagate with a larger velocity, $(1/v_{gi} - 1/v_g)^{-1}$, in the moving frame of the driving laser pulse as the RR wavelengths are in the normal dispersion region of fused silica. This gives rise to the RR generated at the earlier position lagging further behind. As a result, the RR becomes positively chirped, and an asymmetric RR spectrum is formed. The above analysis reveals that the experimentally observed asymmetric structure of RR originates from the positive chirp property of the RR, which is closely related to the accelerated propagation of the laser pulse after nonlinear focus.

In order to identify the above physical picture, the laser pulse is further propagated in the sample in our simulation, and the corresponding time-frequency map at $z = 22.0$ mm is shown in Fig. 6. Two characteristic properties of the RR spectra can be observed. First, the RR spectra generated at the earlier position ($z < 20.0$ mm) lag further behind, and the above-mentioned temporal chirped structure still exists. In addition, a vertical structure is formed, as shown by the dashed rectangle in Fig. 6. These spectra of the vertical structure lag behind, which is also due to the smaller group velocity of the RR with respect to the driving laser pulse. Meanwhile, this vertical structure illustrates that the newly generated RRs at farther propagation positions have almost the same spectra, which can also be understood in the same way as discussed above. More specifically, after the light bullet is formed and the laser-pulse intensity becomes clamped, the time corresponding to the peak intensity changes linearly with respect to propagation distance, as shown by the red dashed line in Fig. 5(a), indicating that the laser pulse propagates with a constant velocity. At this situation, the phase-matching condition is not changed anymore along with light-bullet propagation. As a result, the generated RR spectrum remains invariable. Therefore, the vertical structure in the time-frequency map is also a natural consequence of the propagation dynamics of the light bullet.

IV. CONCLUSION

In summary, we have experimentally and numerically studied the asymmetric structure of RR in the visible region during midinfrared femtosecond laser filamentation in fused silica. Numerical simulation of the laser-pulse propagation in the sample by UPPEs gives results qualitatively consistent with the measurement. It was found that the RR is formed in a very short propagation distance just after nonlinear focus. Furthermore, a time-frequency analysis of the laser electric field was applied at various propagation positions in the media, and it was found that the RR spectra are positively chirped in the time domain, which leads to the experimentally observed asymmetric structure of the RR spectra. Based on the ETWM model, this chirp property of the RR can be ascribed to the varying phase-matching condition of the RR at different laser propagation positions, which is closely related to the accelerative propagation of the light bullet during its formation. Our work offers an effective method to study the temporal dynamics of the light bullet by analyzing the RR spectrum and provides a more comprehensive understanding of femtosecond laser-pulse propagation in condensed media.

ACKNOWLEDGMENTS

This work is supported by the National Key R&D Program of China (Grant No. 2019YFA0307702), the National Natural Science Foundation of China (Grants No. 11527807 and No. 11834015), the Strategic Priority Research Program of the Chinese Academy of Sciences (Grant No. XDB21010400), and the Science and Technology Department of Hubei Province (Grant No. 2020CFA029).

[1] Y. Kodama and A. Hasegawa, *Solitons in Optical Communications* (Clarendon, Oxford, 1995).
[2] U. Keller, Nature (London) **424**, 831 (2003).
[3] X. Liu, D. Popa, and N. Akhmediev, Phys. Rev. Lett. **123**, 093901 (2019).
[4] D. V. Skryabin and A. V. Gorbach, Rev. Mod. Phys. **82**, 1287 (2010).
[5] E. Rubino, J. McLenaghan, S. C. Kehr, F. Belgiorno, D. Townsend, S. Rohr, C. E. Kuklewicz, U. Leonhardt, F. König, and D. Faccio, Phys. Rev. Lett. **108**, 253901 (2012).
[6] T. G. Philbin, C. Kuklewicz, S. Robertson, S. Hill, F. König, and U. Leonhardt, Science **319**, 1367 (2008).
[7] J. C. Travers and J. R. Taylor, Opt. Lett. **34**, 115 (2009).

[8] M. Narhil, B. Wetzel, C. Billet, S. Toenger, T. Sylvestre, J. Merolla, R. Morandotti, F. Dias, G. Genty, and J. M. Dudley, Nat. Commun. **7**, 13675 (2016).

[9] N. Akhmediev and A. Ankiewicz, *Dissipative Solitons: From Optics to Biology and Medicine* (Springer, Heidelberg, 2008).

[10] G. P. Agrawal, *Nonlinear Fiber Optics*, 4th ed. (Academic, San Diego, 2006)

[11] J. M. Dudley, G. Genty, and S. Coen, Rev. Mod. Phys. **78**, 1135 (2006).

[12] A. Hasegawa and F. Tappert, Appl. Phys. Lett. **23**, 142 (1973).

[13] L. F. Mollenauer, R. H. Stolen, and J. P. Gordon, Phys. Rev. Lett. **45**, 1095 (1980).

[14] X. Liu, X. Yao, and Y. Cui, Phys. Rev. Lett. **121**, 023905 (2018).

[15] K. Goda and B. Jalali, Nat. Photonics **7**, 102 (2013).

[16] Y. Silberberg, Opt. Lett. **15**, 1282 (1990).

[17] D. Majus, G. Tamošauskas, I. Gražulevičiūtė, N. Garejev, A. Lotti, A. Couairon, D. Faccio, and A. Dubietis, Phys. Rev. Lett. **112**, 193901 (2014).

[18] C. Brée, I. Babushkin, U. Morgner, and A. Demircan, Phys. Rev. Lett. **118**, 163901 (2017).

[19] R. I. Grynko, G. C. Nagar, and B. Shim, Phys. Rev. A **98**, 023844 (2018).

[20] S. V. Chekalin, A. E. Dormidonov, V. O. Kompanets, E. D. Zaloznaya, and V. P. Kandidov, J. Opt. Soc. Am. B **36**, A43 (2019).

[21] A. Couairon and A. Mysyrowicz, Phys. Rep. **441**, 47 (2007).

[22] P. Béjot, J. Kasparian, S. Henin, V. Loriot, T. Vieillard, E. Hertz, O. Faucher, B. Lavorel, and J.-P. Wolf, Phys. Rev. Lett. **104**, 103903 (2010).

[23] A. Braun, G. Korn, X. Liu, D. Du, J. Squier, and G. Mourou, Opt. Lett. **20**, 73 (1995).

[24] F. Silva, D. R. Austin, A. Thai, M. Baudisch, M. Hemmer, D. Faccio, A. Couairon, and J. Biegert, Nat. Commun. **3**, 807 (2012).

[25] E. A. Stepanov, A. A. Voronin, F. Meng, A. V. Mitrofanov, D. A. Sidorov-Biryukov, M. V. Rozhko, P. B. Glek, Y. Li, A. B. Fedotov, A. Pugžlys, A. Baltuška, B. Liu, S. Gao, Y. Wang, P. Wang, M. Hu, and A. M. Zheltikov, Phys. Rev. A **99**, 033855 (2019).

[26] P. Vasa, J. A. Dharmadhikari, A. K. Dharmadhikari, R. Sharma, M. Singh, and D. Mathur, Phys. Rev. A **89**, 043834 (2014).

[27] M. Durand, K. Lim, V. Jukna, E. McKee, M. Baudelet, A. Houard, M. Richardson, A. Mysyrowicz, and A. Couairon, Phys. Rev. A **87**, 043820 (2013).

[28] J. Darginavicius, D. Majus, V. Jukna, N. Garejev, G. Valiulis, A. Couairon, and A. Dubietis, Opt. Express **21**, 25210 (2013).

[29] C. R. Lourés, T. Roger, D. Faccio, and F. Biancalana, Phys. Rev. Lett. **118**, 043902 (2017).

[30] A. V. Mitrofanov, A. A. Voronin, D. A. Sidorov-Biryukov, S. I. Mitryukovsky, A. B. Fedotov, E. E. Serebryannikov, D. V. Meshchankin, V. Shumakova, S. Ališauskas, A. Pugžlys, V. Ya. Panchenko, A. Baltuška, and A. M. Zheltikov, Optica **3**, 299 (2016).

[31] T. Roger, D. Majus, G. Tamosauskas, P. Panagiotopoulos, M. Kolesik, G. Genty, I. Gražulevičiūtė, A. Dubietis, and D. Faccio, Phys. Rev. A **90**, 033816 (2014).

[32] M. Kolesik, E. M. Wright, and J. V. Moloney, Opt. Express **13**, 10729 (2005).

[33] E. Rubino, A. Lotti, F. Belgiorno, S. L. Cacciatori, A. Couairon, U. Leonhardl, and D. Faccio, Sci. Rep. **2**, 932 (2012).

[34] D. Faccio, A. Averchi, A. Lotti, M. Kolesik, J. V. Moloney, A. Couairon, and P. Di Trapani, Phy. Rev. A **78**, 033825 (2008).

[35] C. Gong, Z. X. Li, L. Q. Hua, W. Quan, and X. J. Liu, Opt. Lett. **41**, 4305 (2016).

[36] E. O. Smetanina, V. O. Kompanets, S. V. Chekalin, A. E. Dormidonov, and V. P. Kandivov, Opt. Lett. **38**, 16 (2013).

[37] N. Akhmediev, and M. Karlsson, Phys. Rev. A **51**, 2602 (1995).

[38] A. V. Husakou and J. Herrmann, Phys. Rev. Lett. **87**, 203901 (2001).

[39] A. Couairon, E. Brambilla, T. Corti, D. Majus, O. de J. Ramírez-Góngora, and M. Kolesik, Eur. Phys. J. Spec. Top. **199**, 5 (2011).

[40] I. H. Malitson, J. Opt. Soc. Am. **55**, 1205 (1965).

[41] L. V. Keldysh, Zh. Eksp. Teor. Fiz **47**, 1945 (1964) [Sov. Phys. JETP **20**, 1307 (1965)].

[42] M. Schultze, E. Bothschafter, A. Sommer, S. Holzner, W. Schweinberger, M. Fiess, M. Hofstetter, R. Kienberger, V. Apalkov, V. S. Yakovlev, M. I. Stockman, and F. Krausz, Nature (London) **493**, 75 (2013).

[43] T. J.-Y. Derrien, N. T.-Dejean, V. P. Zhukov, H. Appel, A. Rubio, and N. M. Bulgakova, arXiv:2104.08971.

[44] A. J. Taylor, G. Rodriguez, and T. S. Clement, Opt. Lett. **21**, 1812 (1996).

[45] A. Kaiser, B. Rethfeld, M. Vicanek, and G. Simon, Phys. Rev. B **61**, 11437 (2000).

[46] M. Durand, A. Jarnac, A. Houard, Y. Liu, S. Grabielle, N. Forget, A. Durécu, A. Couairon, and A. Mysyrowicz, Phys. Rev. Lett. **110**, 115003 (2013).

[47] P. Audebert, Ph. Daguzan, A. Dos Santos, J. C. Gauthier, J. P. Geindre, S. Guizard, G. Hamoniaux, K. Krastev, P. Martin, G. Petite, and A. Antonetti, Phys. Rev. Lett. **73**, 1990 (1994).

[48] J. R. Gulley and W. M. Dennis, Phys. Rev. A **81**, 033818 (2010).

[49] J. R. Gulley, S. W. Winkler, W. M. Dennis, C. M. Liebig, and R. Stoian, Phys. Rev. A **85**, 013808 (2012).

[50] J. R. Gulley and T. E. Lanier, Phys. Rev. B **90**, 155119 (2014).

[51] M. Kolesik, G. Katona, J. V. Moloney, and E. M. Wright, Phys. Rev. Lett. **91**, 043905 (2003).

[52] D. D. Marcenac and J. E. Carroll, Opt. Lett. **18**, 1435 (1993).

[53] S. Varma, Y.-H. Chen, J. P. Palastro, A. B. Fallahkair, E. W. Rosenthal, T. Antonsen, and H. M. Milchberg, Phys. Rev. A **86**, 023850 (2012).

[54] M. B. Gaarde, Opt. Express **8**, 529 (2001).

[55] J. J. Carrera, X. M. Tong, and S.-I Chu, Phys. Rev. A **74**, 023404 (2006).

[56] C. Gong, J. Jiang, C. Li, L. Song, Z. Zeng, J. Miao, X. Ge, Y. Zheng, R. Li, and Z. Xu, Phys. Rev. A **85**, 033410 (2012).